



## Preparation and Performance of a Modified Iraqi Red Kaolin Clay-Based Sorbent for Methylene Blue Removal in Acidic and Basic Solutions

Batool Majid Saeed<sup>1,2</sup>, Mohammed B. Abdul-Kareem<sup>1\*</sup>

<sup>1</sup> Department of Environmental Engineering, College of Engineering, University of Baghdad, Baghdad 10001, Iraq

<sup>2</sup> Environmental Engineering Department, Mustansiriyah University, Baghdad 10001, Iraq

Corresponding Author Email: [m.mohamd@coeng.uobaghdad.edu.iq](mailto:m.mohamd@coeng.uobaghdad.edu.iq)

Copyright: ©2025 The authors. This article is published by IETA and is licensed under the CC BY 4.0 license (<http://creativecommons.org/licenses/by/4.0/>).

<https://doi.org/10.18280/ijdne.200203>

### ABSTRACT

**Received:** 1 January 2025

**Revised:** 8 February 2025

**Accepted:** 17 February 2025

**Available online:** 28 February 2025

#### Keywords:

*methylene blue, modified kaolin, super-sorbents, cetyltrimethylammonium bromide*

In recent years, the removal of dyes from wastewater via adsorption has attracted significant interest, particularly in the development of high-performance and low-cost sorbents that function effectively in both acidic and basic solutions. The goal of the present study was to synthesize a high-performance sorbent by modifying Iraqi red kaolin clay (IRK) with cetyltrimethylammonium bromide (CTAB), exchanging the interlayer of the clay to produce a hydrophobic material (CTAB-IRK) for the elimination of methylene blue (MB). Additionally, the adsorption of MB dye by CTAB-IRK was studied, focusing on the impact of agitation time, sorbent dosage, initial MB concentration, shaker speed, and pH on the adsorption mechanism. M MB removal efficiency remained stable (87.8–98.7%) over a pH range of 2 to 10. The surface modification with CTAB enhanced the hydrophobicity and adsorption capacity of IRK, facilitating MB removal. The optimum removal efficiency (100%) was achieved with an agitation time of 120 min, a dosage of 0.05 g/100 mL, pH 7, a shaker speed of 200 rpm, and an MB concentration of 50 mg/L. The Freundlich isotherm model ( $R^2=0.926$ ) accurately represented the isotherm data with maximum adsorption capacity of 833.33 mg/g, while the pseudo-second-order model was more applicable with kinetic data.

## 1. INTRODUCTION

High dye concentrations in water lead to an increase in chemical oxygen demand (COD) and limit light penetration, negatively impacting aquatic ecosystems [1]. Methylene blue (MB) is a cationic dye used to color cotton and silk, and its presence in water can cause heart problems, shock, and vomiting [2]. The low biodegradability of MB makes its presence in wastewater more harmful, necessitating its removal [3]. MB is a synthetic dye widely utilized across various industries, including textiles, paper, leather, and pharmaceuticals [4, 5]. Several techniques are being developed for eliminating dyes from industrial wastewater biological treatment [6], chemical oxidation [7], coagulation-flocculation [8], membrane processes [9], ion exchange [10], photocatalytic degradation [11] and sorption [12]. Among various treatment methods, sorption stands out as the most commonly used due to its simplicity in design, cost-effectiveness, and environmental friendliness compared to other techniques. However, pH control often increases operational costs due to the need for additional chemicals, equipment, and continuous monitoring. Therefore, preparing sorbents that can effectively function in both acidic and basic conditions can significantly reduce costs in treatment systems. Numerous studies have explored the use of different sorbents to eliminate MB from wastewater such as tea stem [13], molasses waste [14], wheat bran sawdust [15], rice husks [16],

and different types of sludge [17], but all studies worked in specific pH values. Therefore, the development of low-cost sorbents that work effectively across a wide range of pH levels is critically important in industrial wastewater treatment.

In recent decades, scientists have focused their attention on using clay as an inexpensive and readily available sorbent with the possibility of modifying its surface and improving its sorption capabilities to be applied in several fields, especially in wastewater treatment, whether in dyes or to remove other pollutants. Several clays have been utilized as sorbents to eliminate MB from wastewater, including bentonite [18], zeolite [19], and Iraqi red kaolin clay (IRK) [20-22]. IRK can be modified by several methods, including cationic surfactants [1], thermal activation [23], and many other methods have been used to modify IRK in previous studies [24]. Cetyltrimethylammonium Bromide (CTAB), a cationic surfactant, enhances IRK's hydrophobicity and interlayer spacing, facilitating the adsorption of cationic dyes like MB. Therefore, the objectives of this paper are as follows:

- 1) Develop a novel super-sorbent by modifying IRK clay with cetyltrimethylammonium bromide (CTAB) to increase the removal efficiency of MB across a wide pH range (acidic and basic solutions) by converting the hydrophilic nature of IRK into a hydrophobic one.
- 2) Identify the optimal experimental parameters for effective sorption, including agitation time, shaker

speed, pH, MB concentration, and modifying IRK dosage.

- 3) Characterize the IRK properties before and after modification examine to understand the changes in morphology and functionality efficiency.
- 4) Evaluate CTAB-IRK's sorption kinetics and isotherms to gain insight into its potential applications in industrial wastewater treatment.

## 2. EXPERIMENTAL WORK

### 2.1 Materials

In this study, Iraqi natural kaolin (IRK) was obtained from hussainiyat as one pieces of rock. IRK was washed with distilled water (DW) multiple times to eliminate substances and dried in the oven at 105°C to eliminate any remaining moisture. Once dried, IRK was sieved and grinded to obtain granules within the size range of 1000-300µm using sieves manufactured by Restch, Germany. The properties of the IRK were investigated at the Iraqi-German Laboratory at the University of Baghdad (Table 1). MB dye was obtained from the local market and produced by dissolving 1 g of dye in DW to make a stock solution (1000mg/L). The pH of the dye was adjusted using Sodium Hydroxide (NaOH) or Hydrochloric Acid (HCl) with concentration equal to 0.1 M to achieve the desired acidity or basicity for the experiments. The MB concentration was determined utilizing GENESYS 10 UV Scanning at a wavelength of 664nm. On the other hand, CTAB obtained from the local market, was used as a surfactant to modify the IRK clay, converting its hydrophilic surface properties into hydrophobic ones for enhanced sorption efficiency.

**Table 1.** Properties and chemical composition of IRK

Characteristics	Value
Moisture content (%)	12.8
Specific surface area (m <sup>2</sup> /g)	71.49
Density (kg/m <sup>3</sup> )	2710
SiO <sub>2</sub> (%)	46.47
Al <sub>2</sub> O <sub>3</sub> (%)	21.78
Fe <sub>2</sub> O <sub>3</sub> (%)	15.01
MgO (%)	1.26
CaO (%)	0.64
Na <sub>2</sub> O (%)	0.14
K <sub>2</sub> O (%)	1.22
TiO <sub>2</sub> (%)	2.25
- Loss on ignition (L.O.I) =10.72	

### 2.2 Preparation of CTAB-IRK

To develop IRK into a synthetic sorbent, referred to as CTAB-IRK, the samples were initially added to a conical flask containing DW and shaken at 250rpm for a contact time of approximately 120 minutes, allowing the clay to expand and form a homogeneous mixture [25]. After this swelling process, specific amounts of CTAB were added to the mixture in varying dosages (0.05, 0.1, 0.2, 0.3, 0.4, and 0.5g) per 1g of IRK at room temperature (25°C) with stirring rate of 250rpm. The mixture was stirred continuously for an additional 2 hours (Figure 1). The solid particles were washed multiple times with DW to eliminate any unreacted surfactant. The mixture was centrifuged at 3,000rpm for 30 minutes to separate the solid portion. The solid material was dried in an oven at 105°C,

crushed, and sieved to get granules between 300-1000µm. The CTAB-IRK sample that demonstrated the highest removal efficiency for MB in preliminary tests was selected for subsequent experiments.

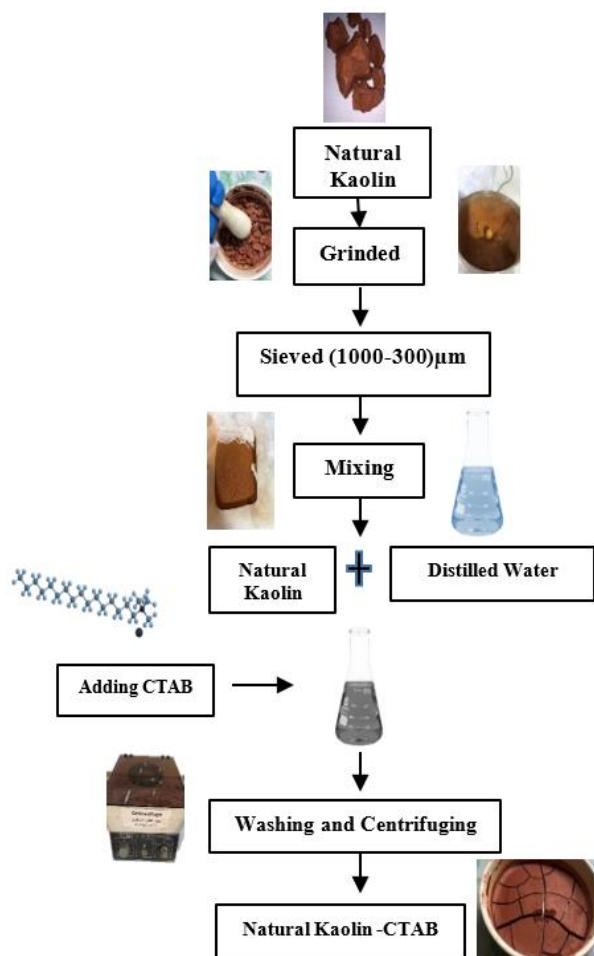


**Figure 1.** Preparation steps of CTAB-IRK

### 2.3 Characterization of CTAB- IRK

Several analyses were conducted to characterize both the IRK and CTAB-IRK. FTIR was used to investigate the functional groups present on the IRK and CTAB-IRK surfaces before and after sorption with wavelength range: 400–4000 cm<sup>-1</sup>. This analysis was performed at the College of Science, University of Baghdad. SEM analysis, using the FEI Company Inspect F50 SEM, was utilized to analysis the surface morphology and observe the structural changes that occurred on the IRK surface after modification with CTAB and the accelerating voltage (15kV), and working distance (10mm). In addition, the surface area of the IRK and CTAB-IRK was determined using Brunauer-Emmett-Teller (BET) analysis with nitrogen gas at 77 K and pressure range (0.05-0.3P/P<sub>0</sub>). This test was carried out at the Department of Refining Researches of the Iraqi Ministry of Oil to assess changes in surface area.

### 2.4 Sorption experiments

To find the removal efficiency of MB dye by CTAB-IRK used batch experiments. The different sorbent dosage of CTAB-IRK (0.01-0.05g/100mL) added to MB dye with initial concentration equal to 300mg/L and stirred with shaker

(Edmund Buhler SM25, German) with range of shaker speed from 0 to 350rpm for agitation time between 0 and 180 min with initial pH (2-10) at 25±3°C (room temperature). At the end of each experiment, MB dye measured by take 10mL from each conical flask and centrifuged (80-1 Tabletop Low-Speed Laboratory Centrifuge, China) at 3,000 rpm for 30 minutes for separation the CTAB-IRK from solution and MB concentration analyzed by using a GENESYS 10 UV Scanning at wave length equal to 664nm. Eq. (1) used to calculate the sorption capacity ( $q_e$ ) of MB dye adsorbed by CTAB-IRK [26]:

$$q_e = \frac{(C_o - C_e)V}{m} \quad (1)$$

where,  $C_o$  and  $C_e$  (mg/L) are the MB initial and equilibrium concentrations, respectively.  $q_e$  is the quantity of the dye that adsorbed by CTAB-IRK per unit mass of CTAB-IRK (mg/g),  $m$  (g) is the CTAB-IRK dosage and  $V$  is the MB solution volume. On the other hand, MB removal efficiency (R%) calculated by using Eq. (2).

$$R (\%) = \frac{(C_o - C_e) \times 100}{C_o} \quad (2)$$

### 2.5 Sorption and kinetic study

The sorption isotherm models were describe the equilibrium state of MB on the surface of CTAB- IRK and applied non-linear forms (Table 2) to fit models with the experimental data [26, 27]. Key parameters include:

1.  $q_{max}$ : The maximum sorption capacity of MB that can be adsorbed by the CTAB-IRK (mg/g).
2.  $1/n$ : Sorption intensity.
3.  $K_F$ : The coefficient of Freundlich model, which provides insights into sorption capacity [27].

The kinetic models were utilized to understand the MB sorption mechanism by CTAB-IRK. The pseudo-first-order and pseudo-second-order models (Table 2) were applied and key parameters include:

1.  $K_1$ : The rate constant of pseudo-first-order ( $\text{min}^{-1}$ ).
2.  $q_t$ : The sorption capacity of MB at any time  $t$  (mg/g).
3.  $K_2$ : The rate constant of pseudo-second-order ( $\text{g mg}^{-1} \text{min}^{-1}$ ).

**Table 2.** The non-linear form of the isotherm and kinetic models

Models	Equation	Reference
Freundlich	$q_e = K_f C_e^{1/n}$	[28]
Langmuir	$q_e = \frac{q_m b C_e}{1 + b C_e}$	[28]
Pseudo-first order kinetic	$q_t = q_e (1 - e^{-k_1 t})$	[29]
Pseudo-second order kinetic	$q_t = \frac{1}{\left(\frac{1}{k_2 q_e^2} + \frac{t}{q_e}\right)}$	[30]

## 3. RESULT AND DISCUSSION

### 3.1 Synthetic CTAB-IRK

Figure 2 illustrates the IRK modification by using varying dosages of CTAB and sorption removal efficiency of MB. In

this experiment, the IRK dosage of was kept constant at 1g, with 300mg/L of MB concentration, pH adjusted to 7, and an agitation speed equal to 250rpm for 110 min at 25±5°C (room temperature). The findings demonstrate that the MB elimination efficiency increased dramatically from 87.56% to 98.53% when the CTAB dose was raised from 0.05g to 0.5g. The highest rate of elimination was obtained at 0.5g, and the sorption efficiency of CTAB-IRK was 1.29 times greater than that of the IRK due to converting the IRK surface from hydrophilic to hydrophobic and increasing the space between the inner layers of IRK [31, 32].

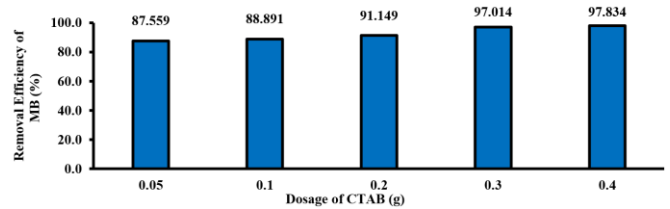


**Figure 2.** The effect of CTAB dosage on aqueous solution content 1 g of IRK and removal of MB sorption ( $C_o=300\text{mg/L}$ , 200rpm,  $t=2\text{hr}$ ,  $\text{pH}=7$ )

### 3.2 Characterization of CTAB –IRK

The characterization of sorbent analysis by using Scanning Electron Microscopy (SEM), Energy Dispersive X-ray Spectroscopy (EDS), Fourier Transform Infrared Spectroscopy (FTIR), and X-ray Diffraction (XRD). The SEM photograph earlier than change discovered that the microstructure surface of IRK includes huge particles organized in abnormal pore stacks with a difficult and more scattered floor, as proven in Figure 3(a), while the morphology of CTAB-IRK with CTAB changed notably after modification, becoming more porous microstructurally regular, containing ordinary-sized holes due to the crystallization that took place, and its floor is smoother because of the coverage [31]. To identify the elements compositions and constituent of IRK and CTAB-IRK was determined by EDS based on comparing the measurement results that got from X-ray intensity ratio which created from the elements of IRK to be tested with the same elements present in the standard IRK. To determine the elements components of IRK, the X-rays characteristics for each element was compared with the standard value, this characteristic refers to the element concentration that present in the sample, the X-ray ionization probability of the element, and the electrons path length. Figures 3(a) and (b) show that the highest EDX elemental distribution peaks were at (O, C, Si, Fe, and Al) elements, because of the alum inosilicate IRK structure. In addition to other elements that present in low quantities were (Mg, Na, Ti, Cl, and K) as shown in Figure 3. The increasing of carbon (C) after the modification process because of the presence of CTAB which attaches to the IRK surface leading to introduce additional carbon atoms and therefore increasing the overall carbon content while it covers some oxygen atoms and reduces the overall percentage of oxygen after the modification process.

The FTIR of CTAB-IRK before and after MB sorption shown in Figure 4, the intensity of the C-H stretching peaks around 2917 $\text{cm}^{-1}$  and 2850 $\text{cm}^{-1}$  has significantly decreased compared to the CTAB- IRK spectrum because of the sorption of MB has led to the partial displacement or covering of the CTAB on the clay surface. The Si-O stretching peak at

1031 $\text{cm}^{-1}$  has shifted to 1030 $\text{cm}^{-1}$  and appears to have a slightly different shape while the Al-OH bending peak at 912 $\text{cm}^{-1}$  has also shifted to 911 $\text{cm}^{-1}$  and shows a slight change in intensity. CTAB is known to intercalate and modify the surface of IRK by exchanging with interlayer cations and interacting with -OH groups on surface of IRK. This modification leads to shifts in FTIR bands because CTAB's long alkyl chain and quaternary ammonium head form new interactions with IRK. In addition, peaks associated with Si-O

and Al-O bonds may also shift slightly because the CTAB molecules affect the electron density around the siloxane framework. These changes suggest that CTAB not only exchanges with native cations but also forms weak electrostatic and van der Waals interactions with IRK, resulting in a more hydrophobic surface and modified pore environment. This enhanced interaction can improve adsorption of MB by increasing the affinity of IRK surface for hydrophobic species [33].

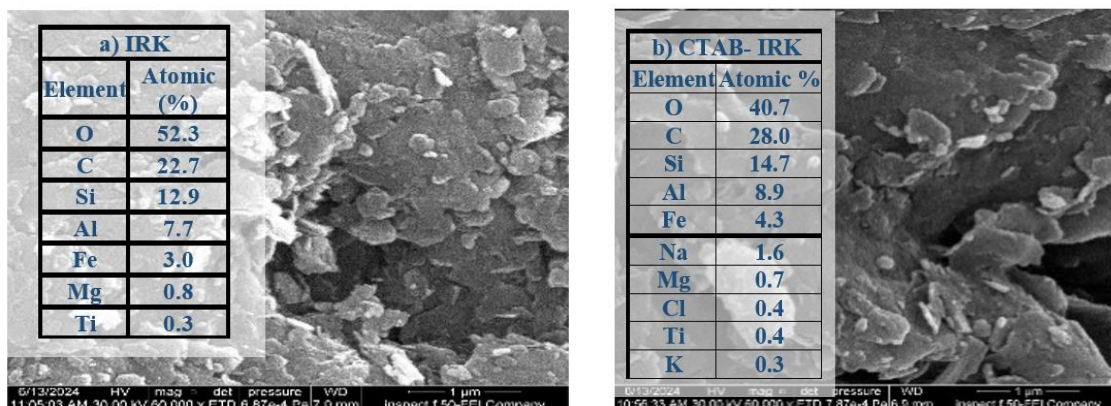


Figure 3. SEM-EDX analysis of a) IRK and b) CTAB-IRK

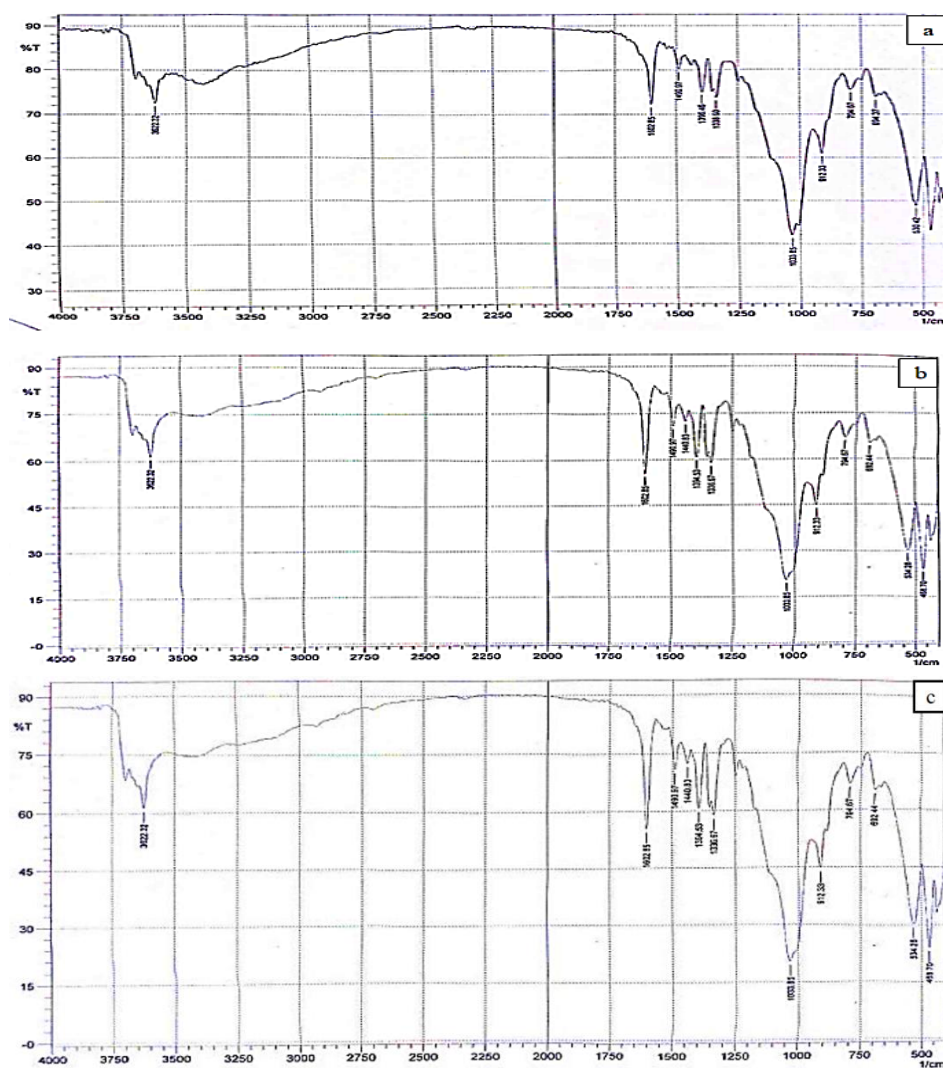
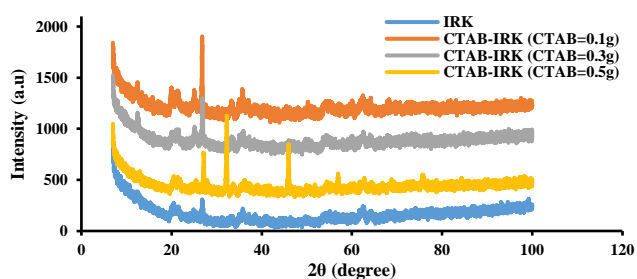


Figure 4. FTIR of (a) IRK, (b) CTAB-IRK, and (c) after sorption MB by CTAB-IRK

On the other hands, these changes indicate that the sorption of MB has caused some structural rearrangements or interactions within the CTAB-modified clay matrix. The addition of MB to the CTAB-modified clay structure resulted in new peaks at 700-800  $\text{cm}^{-1}$ , showing enhanced vibrations and interactions. The fundamental IRK structure is still maintained, as evidenced by the presence of the characteristic clay-related peaks. However, the sorption of MB has led to significant changes in the CTAB-related features. The structural reorganization and new peaks in the lower wavenumber region demonstrate MB's effective sorption on the CTAB-IRK.

The BET investigation findings demonstrated that the specific surface area of the CTAB-IRK ( $55.44\text{m}^2/\text{g}$ ) became less than that of the IRK ( $71.49\text{m}^2/\text{g}$ ) [31]. This is due to the fact that the CTAB penetrated in IRK, covered and interfered with the active sites. In addition, they infiltrated into the inner layers of the IRK structure and connected the channels, decreasing the overall surface area and volume of pores resulting from the modification procedure [34].

To determine the functional groups that appeared on the IRK after CTAB modification, FTIR analysis was conducted in the range of 500–4000 $\text{cm}^{-1}$ . The absorption band on IRK at 3622 $\text{cm}^{-1}$  indicates the presence of O-H stretching and Si-OH (silanol), while the Al-OH groups appear at 3394 $\text{cm}^{-1}$ . Furthermore, the strong bands at 1035, 796, and 692 $\text{cm}^{-1}$  are caused by the existence of the tetrahedral layer Si-O-Si family [35]. Figure 4(b) depicts the CTAB-IRK sample with new absorption bands at 2917 and ~2850 $\text{cm}^{-1}$ , which are not labeled but clearly visible, along with an additional band at 1446 $\text{cm}^{-1}$ . Because of the evaporation of water in the IRK, the -OH band shifted from 1650 $\text{cm}^{-1}$  to a lower frequency of 1637 $\text{cm}^{-1}$  [36]. The new peaks are characteristic of C-H stretching vibrations from the long chain of CTAB. Their existence indicates that CTAB has been properly integrated onto the IRK surface. The presence of  $\text{CH}_3$  and  $\text{CH}_2$  groups after modification confirms the interaction between the surfactant CTAB and the IRK compositions [18]. The analysis results proved that the surfactant successfully modified the natural IRK while maintaining its basic structure unchanged.



**Figure 5.** XRD diffraction pattern for IRK and CTAB-IRK

To analyze the crystalline and amorphous natures by determine the variations in crystalline and phases properties of IRK after the modification process, XRD was used [37]. In general, the significant increase in intensities at  $2\theta$  ( $27.17^\circ$ ,  $32.24^\circ$ , and  $45.95^\circ$ ) in the modified sample because of increased overall crystallinity as shown in Figure 5 while most peak positions remain similar, indicating the basic crystal structure of IRK. The slight peak shift at  $27.17^\circ$  due to changes in d-spacing caused by CTAB. The CTAB modification has enhanced the crystallinity of certain planes in the IRK structure, the most significant change is at  $32.24^\circ$ , which is a

key indicator of the CTAB- IRK interaction while the basic crystal structure of IRK is preserved leading to conclude successful modification by CTAB.

### 3.3 Batch experiments

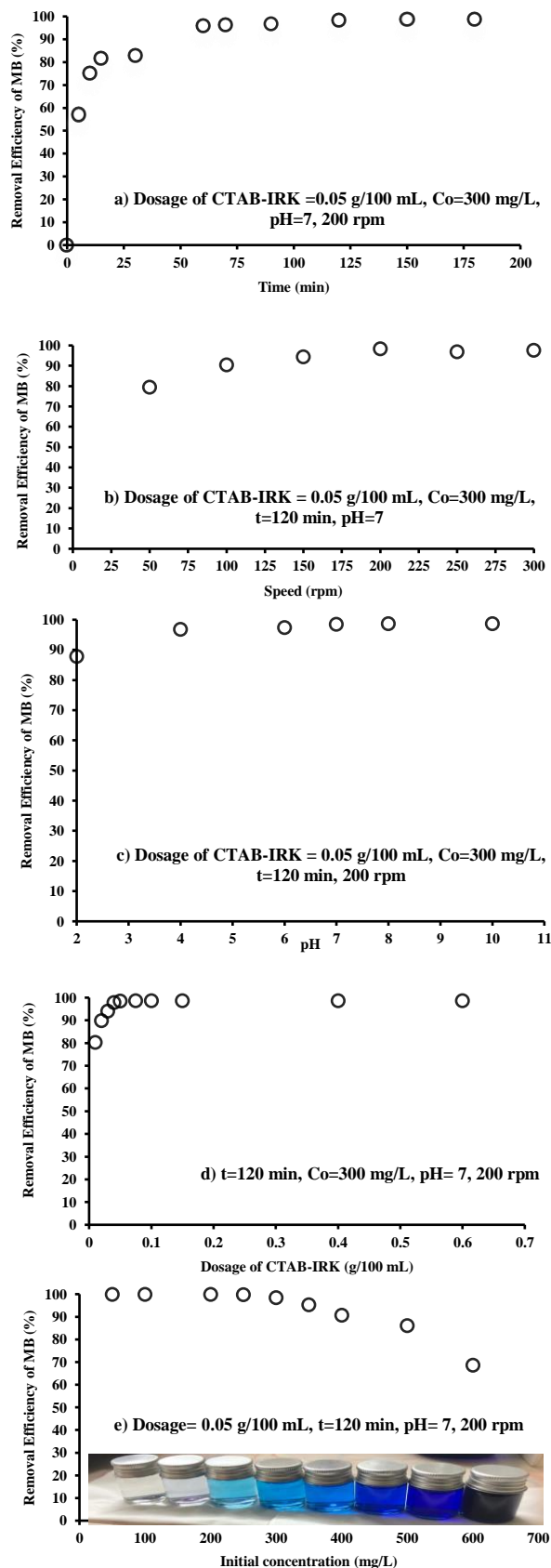


**Figure 6.** The influence of contact (a) time, (b) speed, (c) pH, (d) dosage, (e) MB concentration

Determining the optimal agitation time is important in the sorption MB to know when reach equilibrium. CTAB-IRK (0.05g/100mL) was added to solution content 300mg/L of MB concentration and stirred with agitation speed equal to 200rpm at the range of contact time from 5 to 180 min. The sorption of MB dye by the CTAB-IRK increased as the contact time increased, and the sorption process was rapid at first but then began to slow with the passage of time (Figure 6(a)), owing to the fact that the active sites available on the surface of the sorbent (CTAB-IRK) responsible for the sorption process decrease with time as sites saturated with MB dye reach equilibrium. It was found that 75.205% of MB was removed after the first 5 minutes and that the highest efficiency (98.5%) was obtained at time equal to 120 min, which adopted in the upcoming experiments, after this equilibrium state there is no significant change in the MB concentration [38]. CTAB-IRK increasing the adsorption capacity by 1.3 times compared to natural IRK.

The influence of agitation speed on MB dye sorption by CTAB-IRK (0 to 350 rpm). It was determined (Figure 6(b)) that the removal rate of dye by CTAB-IRK increased as the speed increased due to increasing the agitation speed leads to enhancing the process of diffusion of the MB on the CTAB-IRK surface and boosted binding of MB to active sites on the surface of the CTAB-IRK [27, 39]. The highest removal efficiency (98.387%) of MB was achieved at 200rpm, after which it increased slightly, so it was adopted in the process as it is an economical and effective option.

The pH parameter is important in the solution due to affects the surface properties of the CTAB-IRK and the ions of the MB solution and thus affects the sorption capacity. The impact of the pH on the MB sorption by CTAB-IRK (0.05g) was studied at the range from 2 to 10 and NaOH and HCl (0.1 M) were utilized to adjust pH values. It was noted that when the pH value increased, the sorption efficiency of MB dye by CTAB-IRK increased (Figure 6(c)). After the modification process of IRK by CTAB becomes positive and the sorption process occurs as a result of electrostatic attraction force between the negative surface of the CTAB-IRK and the cationic MB dye. The highest MB removal was achieved at pH equal to 7 [40].

The impact of CTAB-IRK dosage on the MB removal was investigated at different CTAB-IRK dosages with range (0.01 to 0.05) g/100mL and added to the MB solution with concentration equal to 300mg/L and agitation speed equal to 200rpm for 120 min at room temperature. Figure 6(e) shows that the removal efficiency increased from 80.41 to 98.5% by CTAB-IRK as the amount increased from 0.01 to 0.05g/100mL then the removal increases slightly until it became constant due to increase the active site of CTAB-IRK until it reaches a specific point after which the addition of the CTAB-IRK does not affect the sorption process.

Figure 6(f) demonstrates that the MB removal is significantly influenced by the initial concentration ( $C_0$ ) of MB. These efficiencies decreased from 100 to 68.7% as  $C_0$  increased from 50 to 600mg/L, respectively, with a dosage of 0.05g/100mL, a contact time of 120 minutes, a pH of 7, and a shaker speed of 200rpm. At lower concentrations, it is found that all MB will interact with the available binding sites, leading to a substantial increase in sorption efficiency. However, as the concentration rises, the high number of MB may overwhelm the available binding sites, resulting in decreased sorption efficiency [41, 42].

### 3.4 Sorption isotherm and kinetic models

To find the behavior of sorption between the CTAB-IRK and the MB [43], two models were used: Freundlich and Langmuir. Langmuir model is based mainly on the assumption that the maximum sorption capacity can be achieved through a saturated monolayer of MB on the solid surface of the CTAB-IRK at a fixed temperature (homogeneity), while Freundlich model assumes that it is achieved through multilayer MB sorption on the surface of the CTAB-IRK at equilibrium (heterogeneity) [43]. The resulted data were fitted with the isotherm models to find the best coefficient of determination ( $R^2$ ) through the nonlinear fitting by using Excel 2016 as shown in Figure 7(a) and Table 3. The isotherm data showed the best fit with the Freundlich model, which had coefficient of determination (0.926) higher than the Langmuir value of model (0.848). The n value was 9.488 which is in the range ( $1 < n < 10$ ) of favorable sorption process. Table 4 shows a comparison of maximum sorption capacities of MB on various sorbents reported in the literatures. Obviously, that the sorption capacity of CTAB-IRK clay in this research was much higher than that of other sorbents.

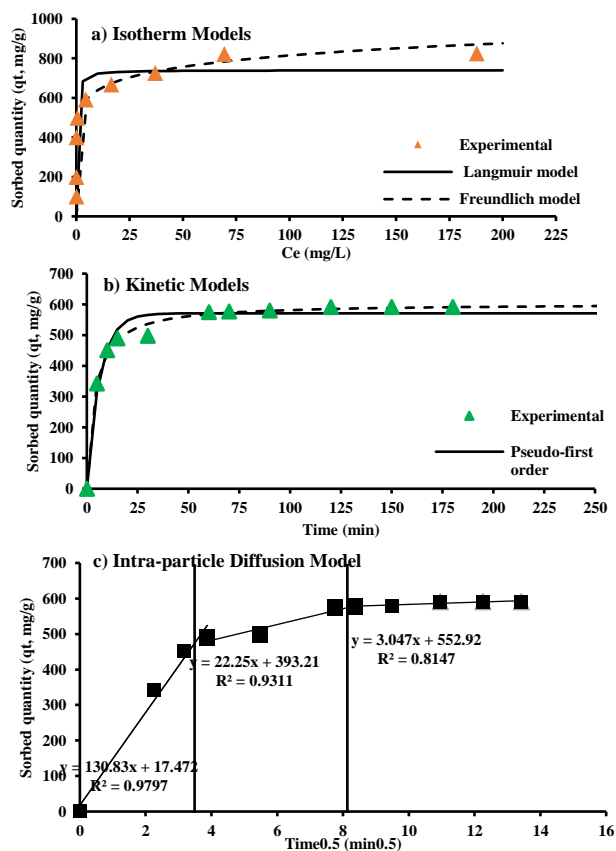


**Figure 7.** Sorption measurements using a) isotherm, b) kinetic, and c) intra-particle diffusion models for sorption of MB by CTAB-IRK

The sorption kinetics of the MB from the solution on the CTAB-IRK surface is considered an important matter, so the kinetic models were adopted are pseudo-first-order and pseudo-second-order models [44, 45]. The pseudo-second order model represents the reaction of the surfactant with the CTAB-IRK because of the experimental capacity  $q_e$  closer to the calculated capacity  $q_c$  than pseudo first order (Figure 7(b)). As listed in Table 3, the pseudo-second-order model achieved

the higher coefficient of determination ( $R^2$ ). So, chemisorption is the mechanism that controls the reaction.

**Table 3.** The constant values of isotherm, kinetic models, and intra-particle diffusion for interaction of MB by CTAB-IRK

Model	Parameter	Value
Freundlich	$K_f$ (mg/g) (L/mg) <sup>1/n</sup>	501.384
	$n$	9.488
	$R^2$	0.926
Langmuir	$q_{max}$ (mg/g)	740.205
	$b$ (L/mg)	4.103
	$R^2$	0.848
Pseudo-first order	$q_e$ (mg/g)	570.733
	$k_1$ (1/min)	0.160
	$R^2$ , SSE	0.975, 7719.95
Pseudo-second order	$q_e$ (mg/g)	603.073
	$k_2$ (g/mg min)	0.00044
	$R^2$ , SSE	0.99, 1768.57
Intra-particle diffusion	Portion 1	
	$k_{int}$ (mg/g min <sup>0.5</sup> ), C	130.83, 17.472
	$R^2$	0.97
	Portion 2	
	$k_{int}$ (mg/g min <sup>0.5</sup> ), C	22.25, 393.21
	$R^2$	0.93
Portion 3		
$k_{int}$ (mg/g min <sup>0.5</sup> ), C	3.047, 552.92	
$R^2$	0.81	

**Table 4.** Sorption capacity of MB by various sorbents

Sorbents	$q_{max}$ (mg/g)	Reference
Tamazert Kaolin	111	[46]
Rice Straw Biochars	131.58	[47]
Algerian kaolin	52.76	[20]
kaolin clay	83	[22]
IRK	240.4	[21]
IKaol	114.94	[24]
CTAB-IRK	833.33	This study

The sorption kinetics were further evaluated using the intra-particle diffusion model, which showed a linear relationship between  $t^{0.5}$  and  $q_t$  with satisfactory  $R^2$  values, as illustrated in Figure 7(c). In this model, the y-axis intercepts indicate that intra-particle diffusion contributes to the sorption of MB, although it is not the rate-limiting step. The plotted lines display three distinct linear segments, suggesting that sorption occurs via multiple processes. The slopes of these lines represent the rate constants ( $k$ ), with higher values observed in 'portion 1' compared to 'portions 2 and 3', as shown in Table 3. This suggests that the initial sorption phase may be driven by rapid external surface sorption mechanisms. The sorption process consists of the following stages:

- 1) The initial phase is bulk diffusion (portion 1), contaminants are transferred from the bulk solution to the bead surface, characterized by external mass transfer.
- 2) The intra-particle diffusion model is portion 2 which involves contaminants diffusing into the pores of the beads.
- 3) Equilibrium stage is the portion 3 and the sorbate concentration between the solution and bead surface reaches equilibrium.

The rate constants for each phase,  $k_1$  and  $k_2$ , were determined from the slopes of the respective linear segments, as detailed in Table 3. Macropore diffusion was found to play

a more significant role than micropore diffusion in the beads. The deviation from the origin point suggests that diffusion imposes a limitation on the overall sorption rate [45-51].

#### 4. CONCLUSIONS

In this study, Iraqi red kaolin clay (IRK) was modified by CTAB to obtain an organoclay that achieved higher sorption efficiency for removing MB dye and this environmentally friendly method enhances the clay's adsorption capacity without the use of hazardous chemicals, aligning with green chemistry principles. The effect of different parameters effect on the sorption process was investigated such as CTAB-IRK dosage, agitation time, MB concentration, agitation speed, and pH. The highest removal of MB dye (100%) achieved at 0.05g/100mL, 120 min, 50mg/L, 200rpm, and pH 7. The experimental data fitted pseudo-second-order and Freundlich for the kinetic and isotherm model with maximum sorption capacity 833.33mg/g. This high sorption capacity suggests its potential applicability in industrial wastewater treatment, particularly for effluents from textile industries where dye contamination is prevalent.

#### ACKNOWLEDGEMENTS

The authors are grateful to the Department of Environmental Engineering, College of Engineering/University of Mustansiriyah for the permission to use the laboratory facilities needed in this study.

#### REFERENCES

- [1] Alkizwini, R.S. (2021). The use of an organo-kaolinite sorbent in a permeable reactive barrier for remediating groundwater contaminated with methylene blue dye: Experimental and theoretical investigation. *Environmental Processes*, 8: 889-910. <https://doi.org/10.1007/s40710-021-00515-1>
- [2] Shanshool, H.A. (2019). Adsorption of methylene blue on prepared charcoal from molasses waste. *Journal of Engineering*, 25(9): 92-104. <https://doi.org/10.31026/j.eng.2019.9.8>
- [3] Badis, D., Benmaamar, Z., Benkortbi, O., Boutoumi, H., Hamitouche, H., Aggoun, A. (2016). Removal of methylene blue by adsorption onto Retama raetam plant: Kinetics and equilibrium study. *Chemistry Journal of Moldova*, 11(2): 74-83. [https://doi.org/10.19261/cjm.2016.11\(2\).10](https://doi.org/10.19261/cjm.2016.11(2).10)
- [4] Abd Ali, Z.T. (2021). Green synthesis of graphene-coated sand (GCS) using low-Grade dates for evaluation and modeling of the pH-Dependent permeable barrier for remediation of groundwater contaminated with copper. *Separation Science and Technology*, 56(1): 14-25. <https://doi.org/10.1080/01496395.2019.1708937>
- [5] Hamidi, A., Atia, D., Rebiai, A., Reghioua, A., Zobeidi, A., Messaoudi, M., Ben Seghir, B., Pohl, P., Simal-Gandara, J. (2024). Investigation of adsorption kinetics and isothermal thermodynamics for optimizing methylene blue adsorption onto a modified clay with cellulose using the response surface approach. *Biomass Conversion and Biorefinery*, 14(18): 22573-22587.

- <https://doi.org/10.1007/s13399-023-04397-1>
- [6] Naji, L.A., Jassam, S.H., Yaseen, M.J., Faisal, A.A., Al-Ansari, N. (2020). Modification of Langmuir model for simulating initial pH and temperature effects on sorption process. *Separation Science and Technology*, 55(15): 2729-2736. <https://doi.org/10.1080/01496395.2019.1655055>
- [7] Jasim, R. A., Salman, R.H. (2024). Use of nano Co-Ni-Mn composite and aluminum for removal of artificial anionic dye Congo red by combined system. *Ecological Engineering & Environmental Technology*, 25(7): 133-149. <https://doi.org/10.12912/27197050/188266>
- [8] Slama, H.B., Chenari Bouket, A., Pourhassan, Z., Alenezi, F.N., Silini, A., Cherif-Silini, H., Oszako, T., Luptakova, L., Golińska, P., Belbahri, L. (2021). Diversity of synthetic dyes from textile industries, discharge impacts and treatment methods. *Applied Sciences*, 11(14): 6255. <https://doi.org/10.3390/app11146255>
- [9] Mishra, S., Cheng, L., Maiti, A. (2021). The utilization of agro-biomass/byproducts for effective bio-removal of dyes from dyeing wastewater: A comprehensive review. *Journal of Environmental Chemical Engineering*, 9(1): 104901. <https://doi.org/10.1016/j.jece.2020.104901>
- [10] Dutta, K., Mukhopadhyay, S., Bhattacharjee, S., Chaudhuri, B. (2001). Chemical oxidation of methylene blue using a Fenton-like reaction. *Journal of Hazardous Materials*, 84(1): 57-71. [https://doi.org/10.1016/S0304-3894\(01\)00202-3](https://doi.org/10.1016/S0304-3894(01)00202-3)
- [11] Hadadi, A., Imessaoudene, A., Bollinger, J.C., Bouzaza, A., Amrane, A., Tahraoui, H., Mouni, L. (2023). Aleppo pine seeds (*Pinus halepensis* Mill.) as a promising novel green coagulant for the removal of Congo red dye: Optimization via machine learning algorithm. *Journal of Environmental Management*, 331: 117286. <https://doi.org/10.1016/j.jenvman.2023.117286>
- [12] Al-Wafi, R., Ahmed, M.K., Mansour, S.F. (2020). Tuning the synthetic conditions of graphene oxide/magnetite/hydroxyapatite/cellulose acetate nanofibrous membranes for removing Cr (VI), Se (IV) and methylene blue from aqueous solutions. *Journal of Water Process Engineering*, 38: 101543. <https://doi.org/10.1016/j.jwpe.2020.101543>
- [13] Joseph, J., Radhakrishnan, R.C., Johnson, J.K., Joy, S.P., Thomas, J. (2020). Ion-exchange mediated removal of cationic dye-stuffs from water using ammonium phosphomolybdate. *Materials Chemistry and Physics*, 242: 122488. <https://doi.org/10.1016/j.matchemphys.2019.122488>
- [14] Abd Ali, Z.T., Naji, L.A., Almuktar, S.A., Faisal, A.A., Abed, S.N., Scholz, M., Naushad, M., Ahamad, T. (2020). Predominant mechanisms for the removal of nickel metal ion from aqueous solution using cement kiln dust. *Journal of Water Process Engineering*, 33: 101033. <https://doi.org/10.1016/j.jwpe.2019.101033>
- [15] Waghchaure, R.H., Adole, V.A., Jagdale, B.S. (2022). Photocatalytic degradation of methylene blue, rhodamine B, methyl orange and Eriochrome black T dyes by modified ZnO nanocatalysts: A concise review. *Inorganic Chemistry Communications*, 143: 109764. <https://doi.org/10.1016/j.inoche.2022.109764>
- [16] Li, H., Budarin, V.L., Clark, J.H., North, M., Wu, X. (2022). Rapid and efficient adsorption of methylene blue dye from aqueous solution by hierarchically porous, activated starbons®: Mechanism and porosity dependence. *Journal of Hazardous Materials*, 436: 129174. <https://doi.org/10.1016/j.jhazmat.2022.129174>
- [17] Faisal, A.A., Naji, L.A. (2019). Simulation of ammonia nitrogen removal from simulated wastewater by sorption onto waste foundry sand using artificial neural network. *Association of Arab Universities Journal of Engineering Sciences*, 26(1): 28-34. <https://doi.org/10.33261/jaaru.2019.26.1.004>
- [18] Lee, T.C., Wang, S., Huang, Z., Mo, Z., Wang, G., Wu, Z., Liu, C., Han, H., Ko, T.H. (2019). Tea stem as a sorbent for removal of methylene blue from aqueous phase. *Advances in Materials Science and Engineering*, 2019(1): 9723763. <https://doi.org/10.1155/2019/9723763>
- [19] Ahmed, M.J., Theydan, S.K., Mohammed, A.H.A.K. (2012). Adsorption of phenol and p-nitrophenol onto date stones: Equilibrium isotherms, kinetics, and thermodynamics studies. *Journal of Engineering*, 18(6): 743-761. <https://doi.org/10.31026/j.eng.2012.06.05>
- [20] Pooladi, H., Foroutan, R., Esmaili, H. (2021). Synthesis of wheat bran sawdust/Fe<sub>3</sub>O<sub>4</sub> composite for the removal of methylene blue and methyl violet. *Environmental Monitoring and Assessment*, 193: 1-17. <https://doi.org/10.1007/s10661-021-09051-9>
- [21] Sinbah, H.J., Khazaal, M.H., Hassen, H.S., Sabah, E. (2023). A comparison of kinetic studies of kaolin clay and rice husks for ciprofloxacin adsorption. *International Journal of Applied Pharmaceutics*, 15(3): 132-137. <https://dx.doi.org/10.22159/ijap.2023v15i3.46495>
- [22] Al Juboury, M.F., Alshammari, M.H., Al-Juhaishi, M.R., Naji, L.A., Faisal, A.A., Naushad, M., Lima, E.C. (2020). Synthesis of composite sorbent for the treatment of aqueous solutions contaminated with methylene blue dye. *Water Science and Technology*, 81(7): 1494-1506. <https://doi.org/10.2166/wst.2020.241>
- [23] Ibrahim, S.M., Abd Ali, Z.T. (2020). Using of modified-bentonite as low-cost sorbent for removal of methylene blue dye from aqueous solution. *Association of Arab Universities Journal of Engineering Sciences*, 27(2): 45-54. <https://doi.org/10.33261/jaaru.2020.27.2.005>
- [24] Alhogbi, B.G., Al Balawi, G.S. (2023). An Investigation of a natural biosorbent for removing methylene blue dye from aqueous solution. *Molecules*, 28(6): 2785. <https://doi.org/10.3390/molecules28062785>
- [25] Al-Rubaie, Z.Y., Faisal, A.A.H. (2025). Adsorption of tetracycline from contaminated water using magnesium-iron layered double hydroxide alginate beads prepared from *Schangania aegyptica* and scrap iron. *Journal of Ecological Engineering*, 26(4): 209-219. <https://doi.org/10.12911/22998993/199820>
- [26] Mouni, L., Belkhir, L., Bollinger, J.C., Bouzaza, A., Assadi, A., Tirri, A., Dahmoune, F., Madani, Remini, H. (2018). Removal of methylene blue from aqueous solutions by adsorption on Kaolin: Kinetic and equilibrium studies. *Applied Clay Science*, 153: 38-45. <https://doi.org/10.1016/j.clay.2017.11.034>
- [27] Jawad, A.H., Abdulhameed, A.S. (2020). Mesoporous Iraqi red kaolin clay as an efficient adsorbent for methylene blue dye: Adsorption kinetic, isotherm and mechanism study. *Surfaces and Interfaces*, 18: 100422. <https://doi.org/10.1016/j.surfin.2019.100422>
- [28] Ethaib, S., Zubaidi, S.L. (2020). Removal of methylene blue dye from aqueous solution using kaolin. *IOP*

- Conference Series: Materials Science and Engineering, 928(2): 022030. <https://doi.org/10.1088/1757-899X/928/2/022030>
- [29] Erasto, L., Hellar-Kihampa, H., Mgani, Q.A., Lugwisha, E.H.J. (2023). Comparative analysis of cationic dye adsorption efficiency of thermally and chemically treated Tanzanian kaolin. *Environmental Earth Sciences*, 82(4): 101. <https://doi.org/10.1007/s12665-023-10782-w>
- [30] Bahemmi, S., Zobeidi, A., Atia, S., Neghmouche Nacer, S., Ghernaout, D., Elboughdiri, N. (2023). Activating illite kaolinite clay with CTAB for adsorbing methylene blue: Isotherms, kinetics, and thermodynamics studies. *Tuijin Jishu/Journal of Propulsion Technology*, 44(5): 2023. <https://doi.org/10.52783/tjjpt.v44.i5.2678>
- [31] Jeeva, M., Yaacob, W.Z.W. (2018). Comparison study on the adsorption of a synthetic textile dye using bentonite and surfactant modified bentonite. *Bulletin of the Geological Society of Malaysia*, 65: 107-117. <https://doi.org/10.7186/bgsm65201812>
- [32] Mohammed, A.K., Hameed, H.F., Rashid, I.M. (2023). Wastewater remediation using activated carbon derived from Alhagi plant. *Desalination and Water Treatment*, 300: 36-43. <https://doi.org/10.5004/dwt.2023.29706>
- [33] Lucas, S., Cocero, M.J., Zetzl, C., Brunner, G. (2004). Adsorption isotherms for ethylacetate and furfural on activated carbon from supercritical carbon dioxide. *Fluid Phase Equilibria*, 219(2): 171-179. <https://doi.org/10.1016/j.fluid.2004.01.034>
- [34] Yagub, M.T., Sen, T.K., Ang, H.M. (2012). Equilibrium, kinetics, and thermodynamics of methylene blue adsorption by pine tree leaves. *Water, Air, & Soil Pollution*, 223: 5267-5282. <https://doi.org/10.1007/s11270-012-1277-3>
- [35] McKay, G., Porter, J.F., Prasad, G.R. (1999). The removal of dye colours from aqueous solutions by adsorption on low-cost materials. *Water, Air, & Soil Pollution*, 114: 423-438. <https://doi.org/10.1023/A:1005197308228>
- [36] Huang, Z., Li, Y., Chen, W., Shi, J., Zhang, N., Wang, X., Li, Z., Gao, L., Zhang, Y. (2017). Modified bentonite adsorption of organic pollutants of dye wastewater. *Materials Chemistry and Physics*, 202: 266-276. <https://doi.org/10.1016/j.matchemphys.2017.09.028>
- [37] Huang, R., Hu, C., Yang, B., Zhao, J. (2016). Zirconium-immobilized bentonite for the removal of methyl orange (MO) from aqueous solutions. *Desalination and Water Treatment*, 57(23): 10646-10654. <https://doi.org/10.1080/19443994.2015.1040849>
- [38] Ogbebor, O.J., Okieimen, F.E., Ogbeifun, D.E., Okwu, U.N. (2015). Organomodified kaolin as filler for natural rubber. *Chemical Industry and Chemical Engineering Quarterly*, 21(4): 477-484. <https://doi.org/10.2298/CICEQ140221003O>
- [39] Xu, C., Cao, L., Lin, B., Liang, X., Chen, Y. (2016). Design of self-healing supramolecular rubbers by introducing ionic cross-links into natural rubber via a controlled vulcanization. *ACS Applied Materials & Interfaces*, 8(27): 17728-17737. <https://doi.org/10.1021/acsami.6b05941>
- [40] Faisal, A.A., Al-Ridah, Z.A., Naji, L.A., Naushad, M., El-Serehy, H.A. (2020). Waste foundry sand as permeable and low permeable barrier for restriction of the propagation of lead and nickel ions in groundwater. *Journal of Chemistry*, 2020(1): 4569176. <https://doi.org/10.1155/2020/4569176>
- [41] Zhou, S., Sato, T., Otake, T. (2018). Dissolved silica effects on adsorption and co-precipitation of Sb (III) and Sb (V) with ferrihydrite. *Minerals*, 8(3): 101. <https://doi.org/10.3390/min8030101>
- [42] Aragaw, T.A., Angerasa, F.T. (2020). Synthesis and characterization of Ethiopian kaolin for the removal of basic yellow (BY 28) dye from aqueous solution as a potential adsorbent. *Heliyon*, 6(9): e04975. <https://doi.org/10.1016/j.heliyon.2020.e04975>
- [43] Shaban, M., Abukhadra, M.R., Shahien, M.G., Ibrahim, S.S. (2018). Novel bentonite/zeolite-NaP composite efficiently removes methylene blue and Congo red dyes. *Environmental Chemistry Letters*, 16: 275-280. <https://doi.org/10.1007/s10311-017-0658-7>
- [44] Markandeya, S., Shukla, S.P., Mohan, D. (2017). Toxicity of disperse dyes and its removal from wastewater using various adsorbents: A review. *Toxicol, Research Journal of Environmental Toxicology*, 11(2): 72-89. <https://doi.org/10.3923/rjet.2017.72.89>
- [45] Anirudhan, T.S., Ramachandran, M. (2015). Adsorptive removal of basic dyes from aqueous solutions by surfactant modified bentonite clay (organoclay): Kinetic and competitive adsorption isotherm. *Process Safety and Environmental Protection*, 95: 215-225. <https://doi.org/10.1016/j.psep.2015.03.003>
- [46] Alardhi, S.M., Mohsen, A.M., Breig, S.J.M., Jabbar, N.M., Alfaker, M.J., Salman, A.D., Kareem, K.O., Abd, A.M., AlJaberi, F.Y. (2024). Response surface methodology for optimizing crude oil desalting unit performance in Iraq. *Chemical Papers*, 78: 9091-9102. <https://doi.org/10.1007/s11696-024-03729-3>
- [47] Ding, Z., Wang, W., Zhang, Y., Li, F., Liu, J.P. (2015). Synthesis, characterization and adsorption capability for Congo red of CoFe<sub>2</sub>O<sub>4</sub> ferrite nanoparticles. *Journal of Alloys and Compounds*, 640: 362-370. <https://doi.org/10.1016/j.jallcom.2015.04.020>
- [48] Zaghouane-Boudiaf, H., Boutahala, M., Sahnoun, S., Tiar, C., Gomri, F. (2014). Adsorption characteristics, isotherm, kinetics, and diffusion of modified natural bentonite for removing the 2, 4, 5-trichlorophenol. *Applied Clay Science*, 90: 81-87. <https://doi.org/10.1016/j.clay.2013.12.030>
- [49] Cheung, W.H., Szeto, Y.S., McKay, G. (2007). Intraparticle diffusion processes during acid dye adsorption onto chitosan. *Bioresource Technology*, 98(15): 2897-2904. <https://doi.org/10.1016/j.biortech.2006.09.045>
- [50] Boukhemkhem, A., Rida, K. (2017). Improvement adsorption capacity of methylene blue onto modified Tamazert kaolin. *Adsorption Science & Technology*, 35(9-10): 753-773. <https://doi.org/10.1177/02636174166684835>
- [51] Wang, K., Peng, N., Sun, J., Lu, G., Chen, M., Deng, F., Dou, R., Nie, L., Zhong, Y. (2020). Synthesis of silica-Composited biochars from alkali-fused fly ash and agricultural wastes for enhanced adsorption of methylene blue. *Science of The Total Environment*, 729: 139055. <https://doi.org/10.1016/j.scitotenv.2020.139055>